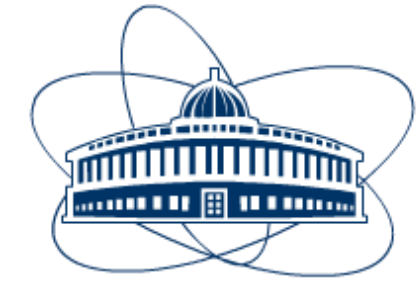

Radiation Protection and the Safety of Radiation Sources

FINAL REPORT ON THE INTEREST PROGRAMME

Wave 14 (02 March - 19 April , 2026)

Submitted By: **Shahd Hassan Rezk**

Alexandria University, Faculty of Engineering

Nuclear And Radiation Department

Supervised by:

Dr Said AbouElazm

Abstract

This report summarizes the practical and theoretical training conducted during the "Radiation Protection and the Safety of Radiation Sources" program. The primary objective was to acquire foundational skills in applied nuclear physics, radiation dosimetry, and shielding. Key laboratory tasks included the energy calibration of a NaI scintillation detector to successfully identify an unknown radioactive source (from the naturally occurring Thorium series), and determining the attenuation coefficients of various shielding materials. Furthermore, the range and energy loss of alpha particles in the air were investigated. Experimental measurements using a pixel detector yielded a practical range of 29 mm, which closely aligned with the theoretical range of 26 mm assessed via Monte Carlo simulations using SRIM software. These results demonstrate a comprehensive understanding of radiation interaction with matter and safety protocols.

Table of Contents

1. Introduction

The safe application of nuclear technologies requires a rigorous understanding of radiation interaction with matter. The primary challenge addressed in this project is bridging the gap between theoretical nuclear physics and practical laboratory applications, specifically overcoming typical experimental uncertainties to accurately identify radioactive sources.

Throughout this training, several milestones were achieved. A gamma scintillation spectrometer was successfully calibrated to identify a naturally occurring radioactive source (Thorium series) despite initial calibration shifts. Additionally, the experimental range of 4 MeV alpha particles was determined to be 29 mm using a pixel detector, which closely aligned with the theoretical range of 26 mm predicted by SRIM Monte Carlo simulations. Finally, the shielding properties of various materials were evaluated, providing a robust foundation for practical radiation safety.

2. Project Goals

The primary objectives of this practical training project are as follows:

1. To perform precise energy calibration of a NaI(Tl) scintillation spectrometer and utilize it to identify the composition of an unknown radioactive source.
2. To calculate and analyze the linear attenuation coefficients of various shielding materials to understand their effectiveness against gamma radiation.
3. To measure the experimental range of 4 MeV alpha particles in the air using a pixel detector.
4. To validate the experimental alpha particle range by comparing it with theoretical data generated through Monte Carlo simulations using SRIM software.

3. Scope of Work

3.1. Used Samples

- An unknown radioactive source, later identified as naturally occurring radioactive material (NORM) from the Thorium-232 decay series.
- An Alpha particle source emitting at approximately 4 MeV.
- Various shielding absorbers (e.g., Lead, Copper, Aluminum) of different thicknesses.

3.2. Equipment

- NaI(Tl) Scintillation Spectrometer for gamma-ray detection.
- Pixel detector (CdTe) for tracking and measuring alpha particle energy and range.
- Personal computer equipped with the ROOT data analysis framework and Microsoft Excel for spectral analysis and curve fitting.
- SRIM (Stopping and Range of Ions in Matter) software for theoretical Monte Carlo simulations.

3.3. Methods

- **Gamma-ray Spectroscopy:** Utilizing energy calibration and internal calibration techniques to accurately identify isotopic signatures despite instrumental gain shifts.
- **Radiation Attenuation:** Applying the Beer-Lambert law to experimental count rates to determine linear attenuation coefficients.
- **Monte Carlo Simulation:** Modeling the interaction of helium ions (alpha particles) with standard dry air to calculate the theoretical stopping range.

4. Results and Discussion

4.1. Data Conversion and Processing

The initial phase of the data analysis required preparing the raw experimental data acquired from the DRS4 evaluation board. The binary files were converted into ASCII format and subsequently structured into ROOT tree formats. This conversion was a crucial preparatory step, enabling the use of the ROOT software framework for advanced spectral visualization, peak fitting, and accurate data extraction.

```python
import struct

binary_filename = "05_Sr90_MIP_ch4_AP704N18_33uC_200V_T21_41_0_7Gss_599ns_20221006s.dat"
text_filename = "output_data.txt"

try:
    with open(binary_filename, "rb") as file:
        binary_data = file.read()

    num_of_values = len(binary_data) // 4

    unpacked_data = struct.unpack(f"{num_of_values}i", binary_data)

    with open(text_filename, "w") as file:
        for value in unpacked_data:
            file.write(f"{value}\n")


except FileNotFoundError:
    print("File Not Found")
except struct.error:
    print("Structure Error")
```

Figure 1: Python Converting Code

```cpp
void plot_data() {
    TH1F *h1 = new TH1F("h1", "Sr-90 Radiation Spectrum;Channels;Counts", 1000, 0, 1000);

    // open file of data after converting
    ifstream file("output_data.txt");
    if (!file.is_open()) {
        cout << "File not Found" << endl;
        return;
    }
    double value;

    while (file >> value) {
        h1->Fill(value);
    }
    file.close();

    // show the spectrum on screen
    TCanvas *c1 = new TCanvas("c1", "Spectrum Canvas", 800, 600);
    h1->Draw();
}
```

Figure 2: C++ Code to Plot the Radiation Spectrum on Root

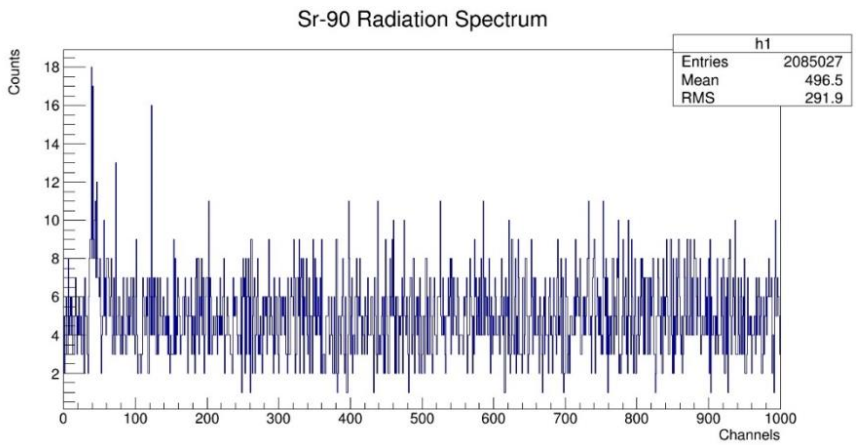

Figure 3: Sr-90 Radiation Spectrum on ROOT

4.2. BGO Scintillation Detector Analysis

4.2.1. Resolution vs. Applied Voltage

To evaluate the operational characteristics of the Bismuth Germanate (BGO) scintillation detector, the energy resolution was investigated as a function of the applied high voltage. The Full Width at Half Maximum (FWHM) was measured for the characteristic photopeaks across a range of voltages. The analysis demonstrated the dependence of detector resolution on the operating voltage, allowing for the determination of the optimal voltage setting required to minimize the FWHM and enhance measurement precision.

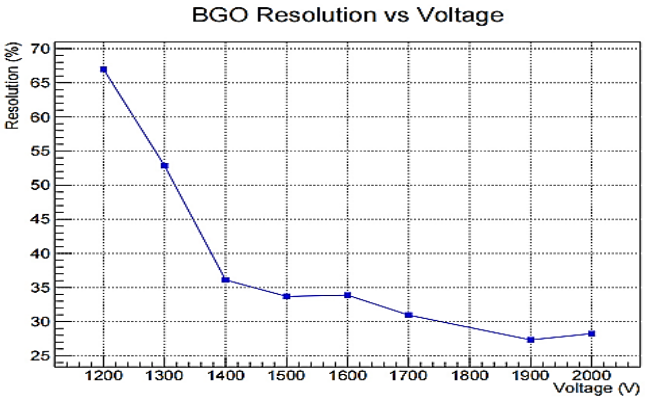

Figure 4: Resolution-Applied Voltage Curve for BGO Detector

Voltage(V)	Mean	Sigma	Resolution(%)	FWHM
1200	1.609	0.458	66.99	1.078
1300	1.355	0.304	52.85	0.716
1400	1.924	0.295	36.11	0.695
1500	2.994	0.428	33.7	1.009
1600	4.401	0.633	33.88	1.491
1700	6.099	0.802	30.96	1.888
1900	10.66	1.237	27.33	2.913
2000	13.67	1.639	28.24	3.86

Table 1: Calculating Resolution of BGO Detector

4.2.2. Energy Calibration

Energy calibration of the BGO detector was performed using standard radioactive sources. A three-point calibration curve was constructed utilizing one photopeak from Cesium-137 (Cs-137) and two photopeaks from Cobalt-60 (Co-60). A linear regression model was applied to the channel-energy data points to derive the specific calibration equation for the BGO detector.

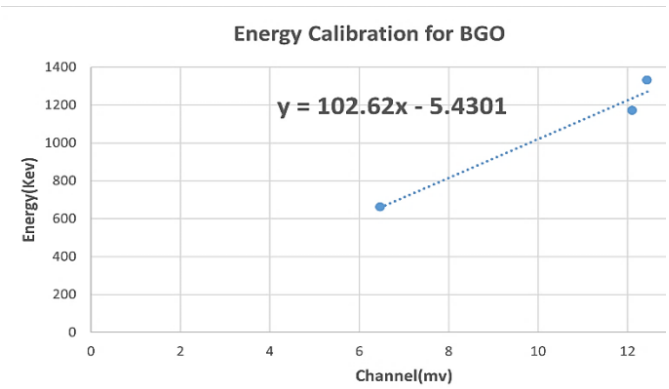

Figure 5: Energy Calibration Curve for BGO detector

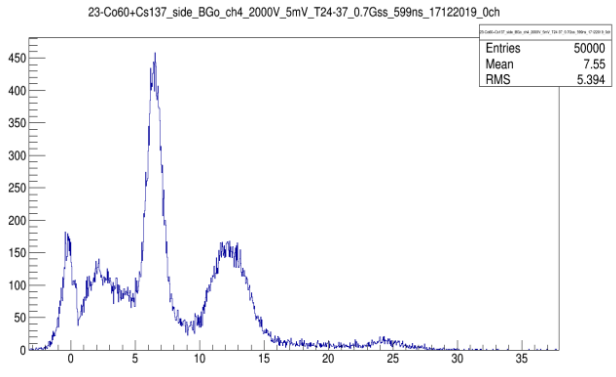

Figure 6: Co60+Cs137 Spectrum for BGO detector on Root

4.3. NaI(Tl) Scintillation Detector Analysis

4.3.1. Resolution vs. Applied Voltage

Similar to the BGO analysis, the energy resolution of the Sodium Iodide (NaI(Tl)) scintillation detector was evaluated across different applied voltages to determine its optimal operating conditions. The FWHM variations were carefully recorded and analyzed to ensure precise spectrometry.

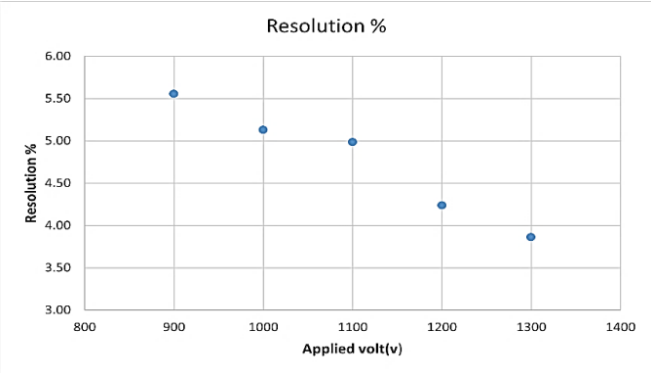

Figure 7: Resolution-Applied Voltage Curve for NaI Detector

Resolution %	FWHM	sigma	mean	volt(v)
5.56	1.48	0.627	26.57	900
5.13	2.33	0.9904	45.46	1000
4.99	3.65	1.552	73.28	1100
4.24	4.60	1.95	108.5	1200
3.86	5.75	2.44	148.8	1300

Table 2: Calculating Resolution of NaI Detector

4.3.2. Energy Calibration

The NaI(Tl) detector was calibrated using the identical standard sources employed previously (Cs-137 and Co-60). The resulting linear calibration curve demonstrated the expected channel-to-energy relationship, confirming the correct setup of the spectrometry system.

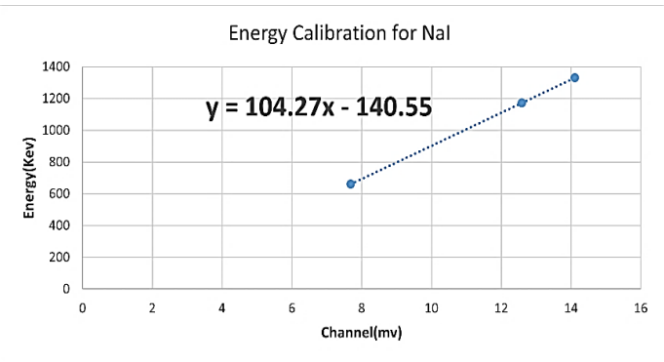

Figure 8: Energy Calibration Curve for NaI detector

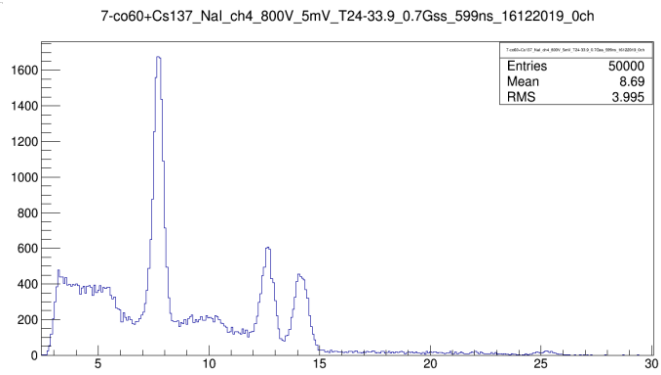

Figure 9: Co-60+Cs-137 Spectrum for NaI detector on Root

4.3.3. Unknown Element Identification

Utilizing the valid NaI(Tl) calibration equation, the spectrum of an unknown radioactive sample was analyzed. The primary gamma energies were calculated from the observed peaks. Cross-referencing these experimental energies with nuclear databases confirmed the presence of Thallium-208 and Actinium-228, which are characteristic daughters of the Thorium-232 decay

series. Thus, the unknown sample was successfully identified as a Naturally Occurring Radioactive Material containing Thorium.

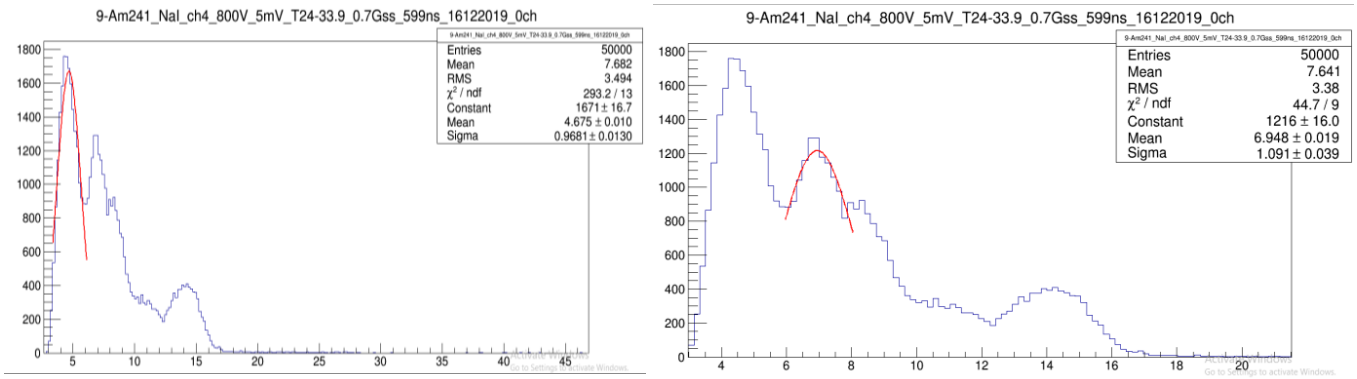

Figure 10: Root Fit for the Two Peaks of the Spectrum of the Unknown Element

346.91225
583.91796

Table 3: Calculated Peak Energies

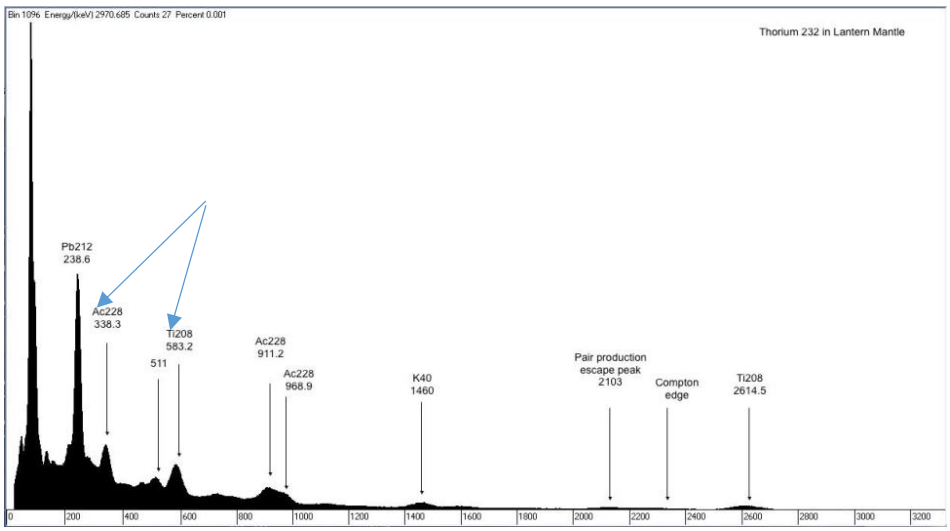

Figure 11: Thorium-232 Gamma Spectrum

4.3.4. Comparison between BGO and NaI(Tl)

A brief comparative analysis between the BGO and NaI(Tl) detectors revealed distinct operational characteristics. While the BGO detector generally offers higher stopping power and efficiency due to its higher density and effective atomic number, the NaI(Tl) detector typically provides superior energy resolution, making it more suitable for identifying closely spaced gamma peaks.

4.4. CdTe Semiconductor Detector Analysis

4.4.1. Energy Calibration and Resolution

A high-resolution Cadmium Telluride (CdTe) semiconductor detector was utilized to analyze low-energy gamma and X-ray spectra. Energy calibration was systematically conducted using standard sources of Americium-241 (Am-241) and Cobalt-57 (Co-57). Following the successful calibration, the detector's energy resolution was calculated for these specific photopeaks. The results highlighted the CdTe detector's exceptional resolving power for closely spaced, low-energy emissions compared to traditional scintillation detectors.

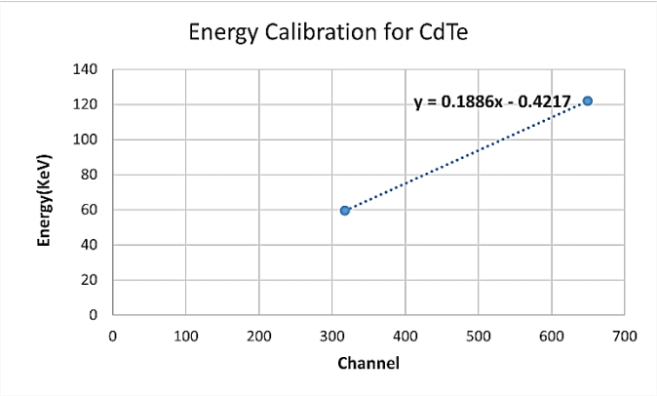

Figure 12: Energy Calibration Curve for CdTe detector

Resolution%	FWHM	sigma	Channel	Energy(Kev)	isotope
1.62	5.1324	2.184	317.7	59.5	Am-241
1.34	8.71145	3.707	649.6	122.1	Co-57

Table 4: Calculating Resolution for Am-241 and Co-57

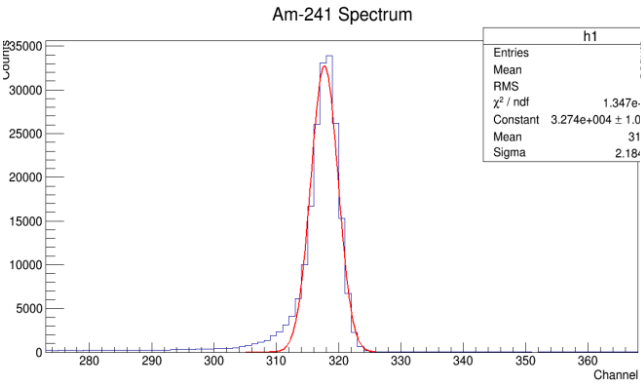

Figure 13: Am-241 Spectrum for CdTe detector on Root

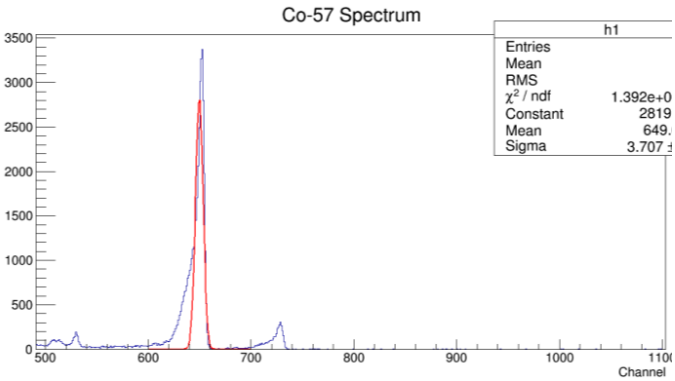

Figure 14: Co-57 Spectrum for CdTe detector on Root

4.5. Linear Attenuation Coefficients

This phase of the experiment aimed to determine the linear attenuation coefficients μ of Aluminum (Al) and Copper (Cu) shielding materials. A BGO detector was used in conjunction with a Cesium-137 (Cs-137) gamma-ray source. The transmitted intensity of the 662 keV gamma rays was measured through varying thicknesses of the absorbers. By applying the Beer-Lambert law ($I = I_o e^{-\mu x}$), the natural logarithm of the transmitted intensity was plotted against the absorber thickness. The slope of the resulting linear fit provided the experimental linear attenuation coefficients for both materials, demonstrating their respective shielding effectiveness against gamma radiation.

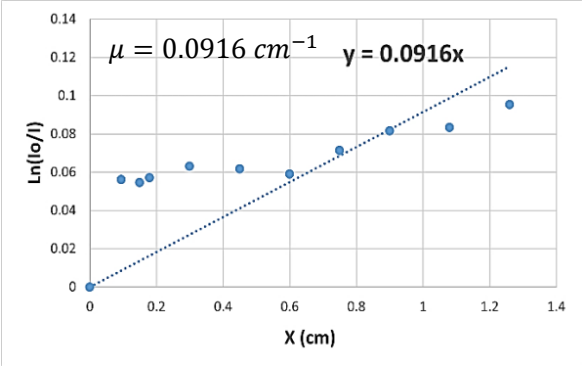

Figure 15: The natural logarithm of the transmitted intensity against the absorber thickness of **Al**

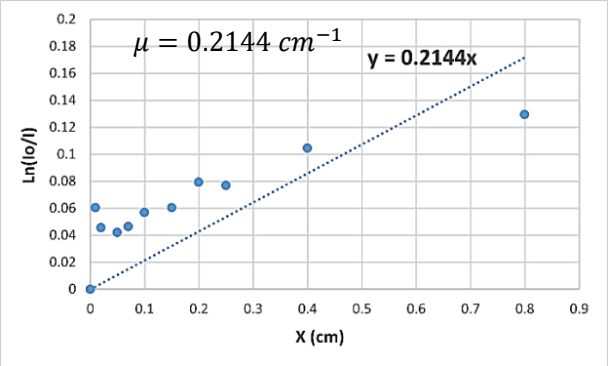

Figure 16: The natural logarithm of the transmitted intensity against the absorber thickness of **Cu**

4.6. Alpha Particle Range Analysis

4.6.1. Experimental Measurement

The practical range of alpha particles in the air was determined by measuring the remaining energy of the particles at various distances from the source using a pixel detector. As the distance increased, the detected energy decreased linearly due to energy loss in the air. A linear fit was applied to the experimental data (E = -127.01x + 3708.5). The practical range was extrapolated to the point where the particle loses all its kinetic energy (E = 0), yielding a total experimental stopping distance of 29 mm.

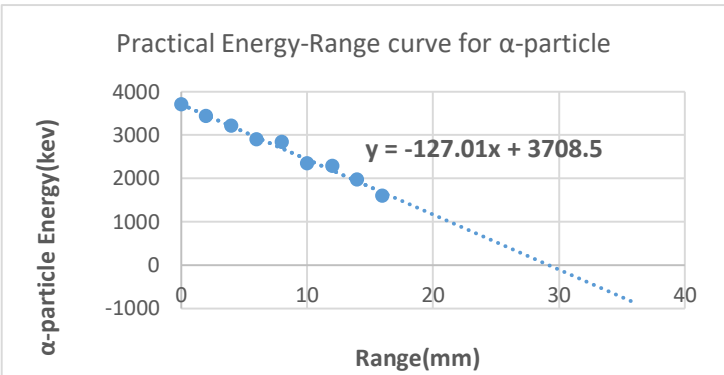

Figure 17: Practical Energy-Range curve for alpha-particle in air

α-particle Energy(kev)	practical range (mm)
3694	0
3432	2
3204	4
2897	6
2835	8
2340	10
2281	12
1962	14
1587	16
0	29

Table 5: He Range in Pixel Detector in air

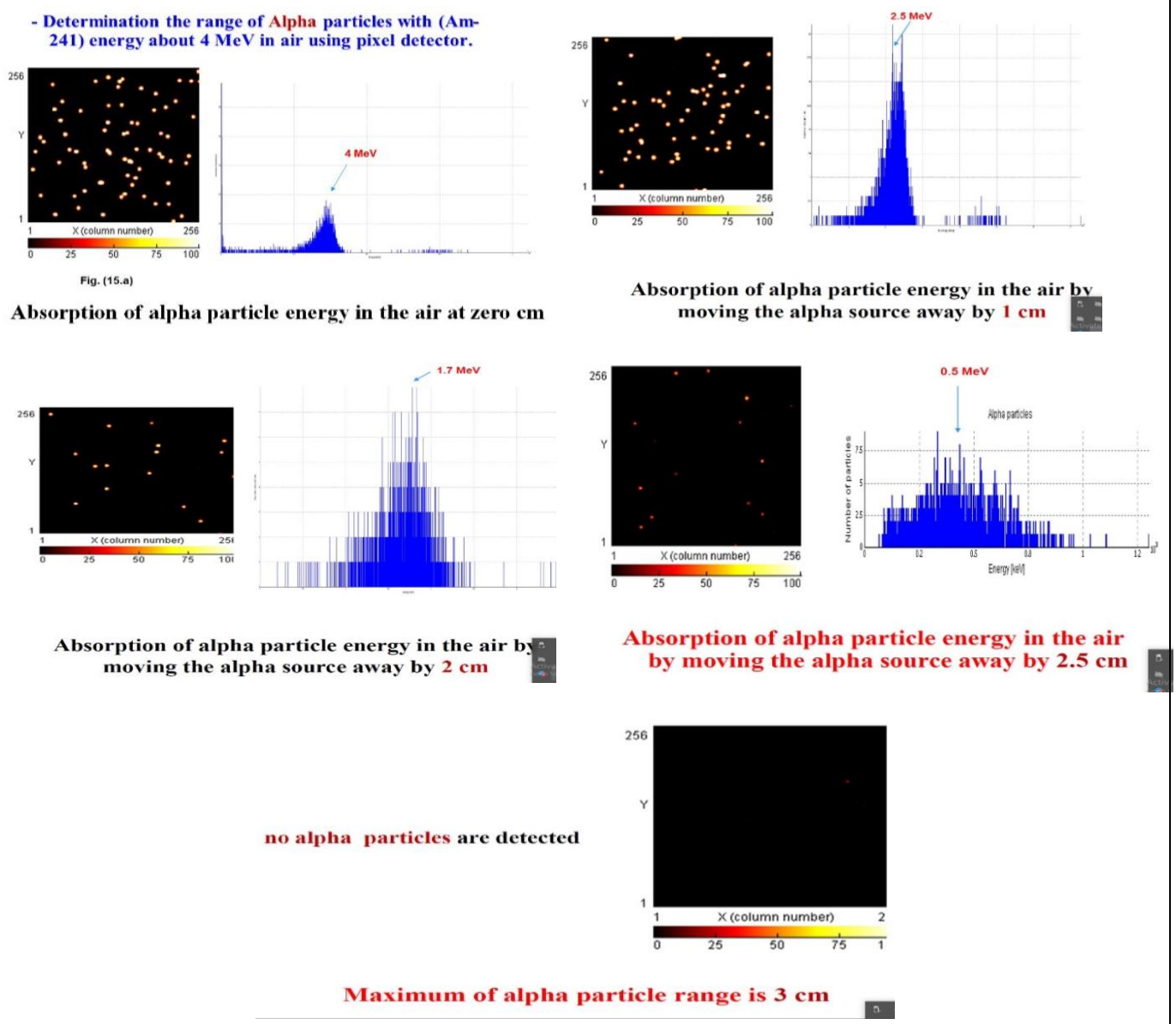

Figure 18: Absorption of alpha-particles in air at Different Distances between the Source and the Detector

4.6.2. Monte Carlo Simulation (SRIM) and Comparison

To evaluate the experimental results, a theoretical model was generated using the SRIM software, which calculates the total stopping range in standard dry air for various initial energies. The theoretical curve plots the required initial energy against the total expected range. Based on the SRIM data, an alpha particle with an initial energy of 4000 keV has a theoretical range of 26 mm.

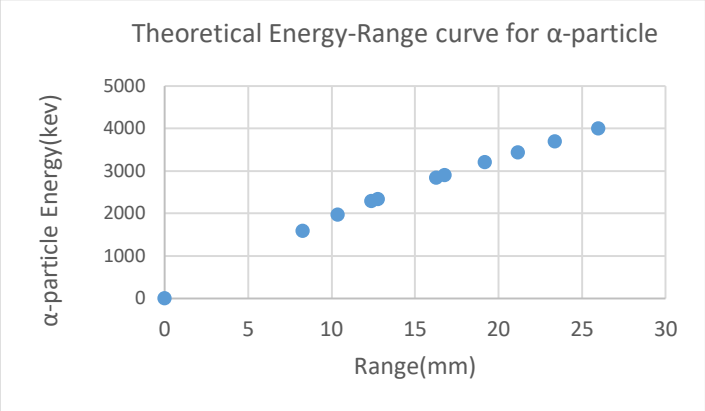

Figure 19: Theoretical Energy-Range curve for alpha-particle in air

α-particle Energy(kev)	theoretical range (mm)(SRIM)
4000	26
3694	23.4
3432	21.2
3204	19.2
2897	16.8
2835	16.3
2340	12.8
2281	12.4
1962	10.4
1587	8.29
0	0

Table 6: He Range in air Theoretically using SRIM

While the practical curve represents the remaining energy versus distance traveled, the theoretical curve represents the initial energy versus total stopping range. Comparing the final stopping points reveals a slight variance (29 mm experimental vs. 26 mm theoretical). This difference is attributed to non-ideal laboratory conditions (e.g., air humidity and pressure deviations from standard dry air), energy attenuation in the detector's thin protective window, and the linear extrapolation method, which simplifies the non-linear energy deposition pattern typically observed at the end of the particle's track (Bragg Peak).

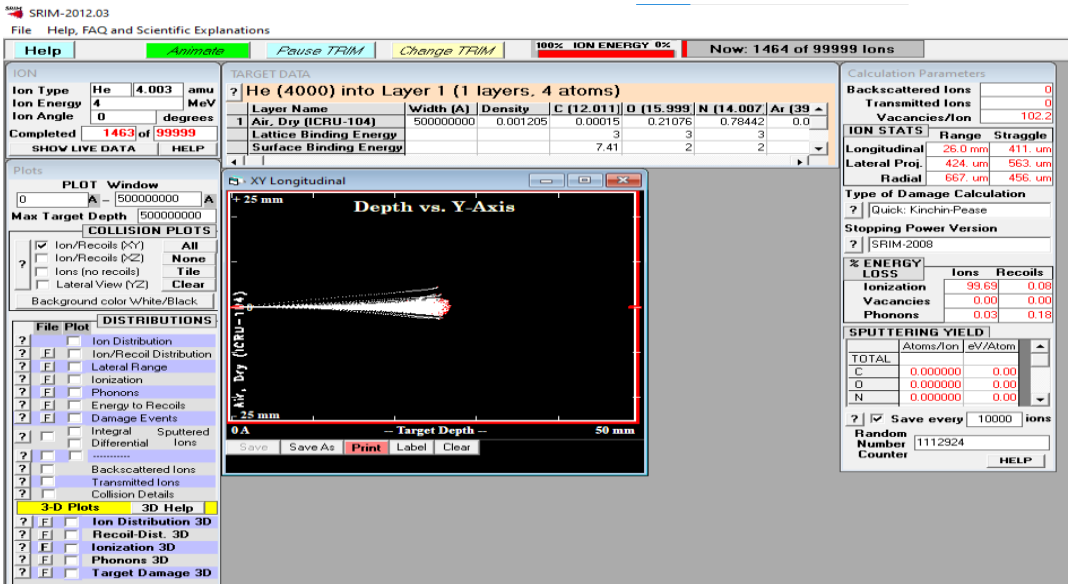

Figure 20: Monte Carlo Simulation on SRIM for Alpha particle with 4MeV Energy

5. Conclusion

This practical training project successfully bridged theoretical nuclear physics concepts with practical laboratory applications. Through a series of comprehensive experiments, extensive hands-on experience was gained in the operation, calibration, and data analysis of various radiation detectors, including BGO, NaI(Tl), and CdTe spectrometers.

The experiments effectively demonstrated the relationship between applied high voltage and detector energy resolution, allowing for precise system optimization. The critical impact of instrumental parameters was highlighted when an induced gain shift was appropriately identified, demonstrating the necessity of strict experimental control. Furthermore, the successful identification of a Thorium-232 NORM sample using the calibrated NaI(Tl) detector showcased the practical utility of these spectroscopic techniques in unknown source identification.

Additionally, the linear attenuation coefficients for Aluminum and Copper were accurately determined, reinforcing fundamental radiation shielding principles. Finally, the practical measurement of the alpha particle range in the air (29 mm) and its subsequent validation using SRIM Monte Carlo simulations (26 mm) provided a profound understanding of particle interactions with matter. The slight variance successfully illustrated the differences between real-world experimental constraints and idealized theoretical models.

Overall, the foundational skills and analytical problem-solving capabilities acquired throughout this training form a robust basis for advanced work in radiation protection and the safety of radiation sources.

6. References

1. Cember, H., Introduction to Health Physics, 3rd Edition, McGraw-Hill, New York (2000).
2. Attix, F.H., Introduction to Radiological Physics and Radiation Dosimetry, Wiley, New York (1986).
3. Martin J.E., Physics for Radiation Protection, Wiley-VCH Verlag Gmbh; Co KGaA, Weinheim (2013).